Unbinding Pathways of an Agonist and an Antagonist from the 5-HT_3 Receptor

A. J. Thompson,* P.-L. Chau,† S. L. Chan,‡ and S. C. R. Lummis*
*Department of Biochemistry, University of Cambridge, Cambridge, United Kingdom; †Bioinformatique Structurale, Institut Pasteur, Paris, France; and ‡Chemical Computing Group, Montreal, Canada

ABSTRACT The binding sites of 5-HT_3 and other Cys-loop receptors have been extensively studied, but there are no data on the entry and exit routes of ligands for these sites. Here we have used molecular dynamics simulations to predict the pathway for agonists and antagonists exiting from the 5-HT_3 receptor binding site. The data suggest that the unbinding pathway follows a tunnel at the interface of two subunits, which is ~8 Å long and terminates ~20 Å above the membrane. The exit routes for an agonist (5-HT) and an antagonist (granisetron) were similar, with trajectories toward the membrane and outward from the ligand binding site. 5-HT appears to form many hydrogen bonds with residues in the unbinding pathway, and experiments show that mutating these residues significantly affects function. The location of the pathway is also supported by docking studies of granisetron, which show a potential binding site for granisetron on the unbinding route. We propose that leaving the binding pocket along this tunnel places the ligands close to the membrane and prevents their immediate reentry into the binding pocket. We anticipate similar exit pathways for other members of the Cys-loop receptor family.

INTRODUCTION

The 5-HT_3 receptor is a member of the Cys-loop ligand-gated ion channel family, which also includes nicotinic acetylcholine (nACh), glycine, and γ-aminobutyric acid type A ($GABA_A$) receptors. These proteins are responsible for fast synaptic transmission, and are the targets of many neuroactive drugs. Similar to other members of the Cys-loop family, the 5-HT_3 receptor forms a pentameric arrangement of subunits (Fig. 1). Each subunit contains an extracellular region and a transmembrane region. The transmembrane region consists of four membrane-spanning α-helices, M1–M4; the M2 segments from each of the five subunits forms the lining of the central ion-conducting pore. A large loop between M3 and M4 constitutes the majority of the intracellular mass of the protein and is responsible for receptor modulation and channel conductance. The extracellular region contains the ligand binding site, and there have been numerous studies to identify the amino acids responsible for receptor-ligand interactions. However, molecular details of the complete receptor structure are still relatively undefined. This is largely because no high-resolution (x-ray crystallographic) structures of Cys-loop receptors have yet been elucidated. Nonetheless, the structure of a protein homologous to the extracellular domain of the nACh receptor, the acetylcholine binding protein (AChBP), has been resolved to 2.1 Å (1–3). This structure has proved useful for homology models of this domain both in the nACh receptor and for other Cys-loop receptors, and comparison with electron microscope data from the nACh receptor has indicated that movement in this domain may trigger receptor gating (4).

Models and mutagenesis studies have shown that the binding site for agonists and antagonists lies between the faces of two adjacent subunits and is formed by the convergence of three loops (A–C) from the principal subunit and three loops (D–F) from the adjacent or complementary subunit. Key residues in these loops in the homomeric 5-HT_{3A} receptor have been identified. As in all Cys-loop receptors, the binding pocket of the 5-HT_3 receptor contains a large proportion of aromatic residues, reminiscent of the active site of acetylcholinesterase (whose structure was resolved to 2.8 Å in 1991), which is located at the bottom of a gorge lined by aromatic residues (5). The gorge residues are considered to provide a rapid yet specific entry pathway for acetylcholine. However, the entry and exit route(s) in the Cys-loop receptor family have not yet been elucidated. This information is of considerable importance, as the route of neurotransmitter entry and/or exit has the potential to be a site of action of neuroactive drugs, and mutations in amino acids in the pathway could be responsible for receptor malfunction. Early electron microscope images of the nACh receptor studies showed the presence of ''tunnels'' between the large extracellular vestibule of the receptor and the synaptic space, suggesting that the neurotransmitter entry and/or exit route(s) may be via the extracellular vestibule (6). However, the current structural data do not support this hypothesis (4). The aim of our work was to determine the exit route for the 5-HT_3 receptor, a typical Cys-loop receptor, using molecular dynamics simulations combined with functional data.

Molecular dynamics simulations have been used to explore a variety of ligand-receptor interactions over the last decade (7,8), with ''steered'' molecular dynamics developed specifically to simulate ligand unbinding from the receptor (9). This method has been applied to various ligand-receptor systems (10–12), for example, to examine unbinding of the

Submitted June 24, 2005, and accepted for publication November 9, 2005.

Address reprint requests to P.-L. Chau, Bioinformatique Structurale, Institut Pasteur, 75724 Paris, France. E-mail: pc104@pasteur.fr.

0006-3495/06/03/1979/13 $2.00

doi: 10.1529/biophysj.105.069385

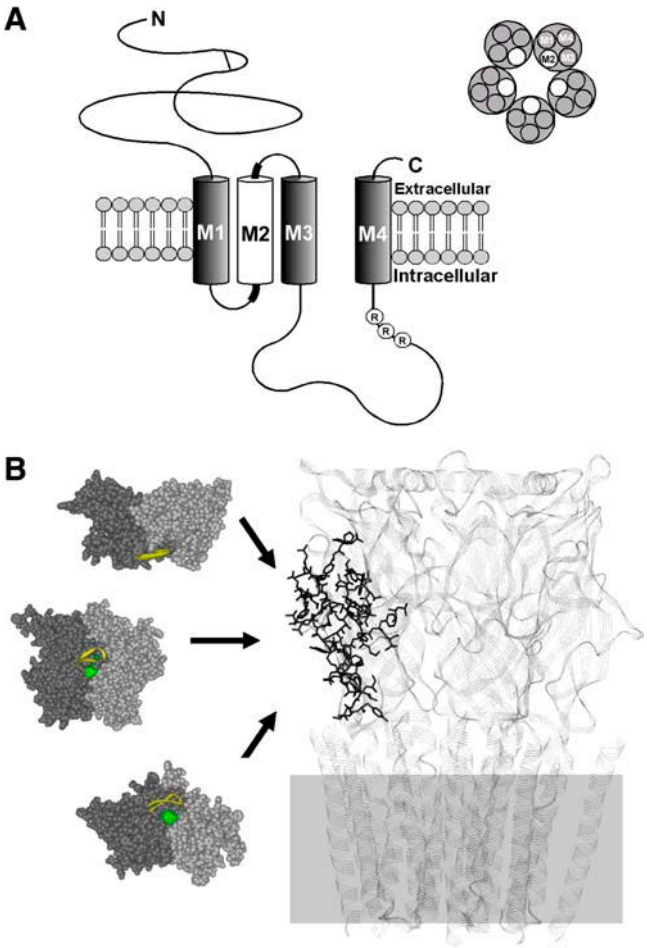

FIGURE 1 Schematic representation of the 5-HT_3 receptor and the location of amino acid residues within the proposed ligand unbinding pathway. (*A*) The cartoon shows features of a typical 5-HT_3 subunit. The residues associated with ligand binding lie between the extracellular N-terminus and the first transmembrane-spanning region (M1). Attention has also been drawn to the residues that line the channel pore (*white cylinder*), those associated with selectivity (*black lines either side of M2*), and those that are associated with channel conductance (®-®-®). The diagram at the upper right is a cross section of the channel shown from above and demonstrates how five subunits associate to form the central ion-conducting pore. (*B*) Residues implicated in unbinding have been superimposed onto a 5-HT_3 homology model that includes the extracellular and transmembrane domains, but omits the intracellular loop. The position of the membrane is shown as a light gray box. Images of bound 5-HT (*green*) from the top, front, and base of the binding site are shown as viewed from the direction of the arrows. 5-HT binds at the interface of two adjacent subunits. For clarity, only two of the five subunits required to create a functional receptor are shown and have been colored in different shades of gray. The C-loop is superimposed in yellow.

streptavidin-biotin complex where the authors identified conformational changes of biotin during the unbinding process and the breaking of hydrogen bonds between the ligand, the receptor, and some surrounding water molecules (13). However, this method requires the predetermination of the unbinding trajectory, which is not always possible. To overcome this problem, the mutual repulsion method was developed to allow the ligand to explore its own unbinding trajectory (14). Here, the distance between the centers of mass of the ligand and the receptor is incrementally increased during the course of the simulation, but the method does not stipulate the exact pathway. This prevents the imposition of a specific trajectory of the unbinding process and allows the ligand to explore the space available and locate its own optimum unbinding trajectory. In this study, we have used this method to locate the unbinding pathway of both an agonist (5-HT) and an antagonist (granisetron) from their binding sites in the 5-HT_3 receptor into the extracellular surroundings.

METHODS

Protein model

A high-resolution structure of the 5-HT_3 receptor is not yet available, but the molecular details of AChBP, a protein homologous to the extracellular domain of this and other Cys-loop ligand-gated ion channel family members, have been resolved (2). We used this structure to create a homology model as previously described (15). Briefly, the three-dimensional model of the 5-HT_3 receptor extracellular domain based on the structure of AChBP was built using MODELLER (16). Sequence alignment was obtained using the program FUGUE. The model was energy-minimized in SYBYL using the AMBER force field. The protein model has 5958 atoms, and it is a cylinder of approximate dimensions 62 × 80 Å.

Modified mutual repulsion simulation

Details of this method have been described previously (14). In the mutual repulsion method, the centers of mass of the ligand and the receptor are assigned what can be called ''pseudocharges'', g, that increase linearly with time. A potential $\Psi(\boldsymbol{r})$ is defined:

$$\Psi(\mathbf{r}_i) = \frac{g^2}{|\boldsymbol{R}_1 - \boldsymbol{R}_2|}, \quad (1)$$

where $\boldsymbol{r}_i$ is the position vector of the atom i, g is the magnitude of the pseudocharge at that time, $\boldsymbol{R}_1$ is the position vector of the center of mass of the receptor, and $\boldsymbol{R}_2$ is that of the center of mass of the ligand.

The pseudocharges interact with each other, but do not affect the normal electronic partial charges assigned to each atom. They repel or attract each other under rules similar to those for normal electronic partial charges. This method approaches the problem of unbinding as a rare event with a large energy difference between the bound and the unbound states. The $\Psi(\boldsymbol{r}_i)$ potential artificially reduces this energy difference so that the transition from one state to another is facilitated. In addition, there are two advantages of the method. First, since the force due to the pseudocharges is calculated with respect to the centers of mass, no torque is generated on the molecules. The molecules will be allowed to explore the unbinding path with fewer artificial forces. Second, since the pseudocharge increases slowly, the potential $\Psi(\boldsymbol{r}_i)$ can be exploited for the calculation of the Helmholtz free energy by the adiabatic switching method.

The position of 5-HT in the 5-HT_3 receptor is shown in Fig. 1. The only discernible opening in the extracellular domain is located toward the base of the ligand binding site, and thus the force was directed to push the ligand out of its binding site in this direction (z direction), although in some simulations the direction was varied to ensure this did not bias the data. The protein was centered with its fivefold axis of symmetry coincident on the z axis, with its extracellular side in the negative z direction and its membrane side in the positive z direction. A point directly above the ligand in the negative z direction was then used as the center of repulsion. The force on the protein was artificially reduced to zero to prevent the receptor from spinning.

Simulation details

All simulations were carried out using a modified form of the DL_POLY molecular dynamics simulation package (17) (see also http://www.cse.clrc.ac.uk/msi/software/DL_POLY/), which incorporated the mutual repulsion method. The CHARMm22 potential was used throughout (18). The cut-off for the nonbonded interactions was 10 Å, as used previously (11).

Two series of simulations were carried out. The first was initiated using an agonist (5-HT) docked into the binding site (15), and the second was initiated with an antagonist (granisetron) docked into the same site (19). In each simulation, the structure of the protein-ligand complex was minimized for 20,000 steps using the zero-K minimization method. All nonhydrogen atoms of the ligand and all C_α atoms of the protein were tethered to their original positions using a harmonic potential. The structure with 5-HT bound was heated to 310 K over 250 ps, followed by an equilibration period of 100 ps. The granisetron-bound structure was heated to 310 K over 100 ps, followed by an equilibrium period of 50 ps.

Two starting conditions were used after equilibration to examine their effect on the final unbinding trajectory. In the first set of conditions, the unbinding simulation continued from equilibration (no velocity rescaling), and in the second set of conditions the velocities of all particles were rescaled to 310 K at the beginning of the data production run (initial velocity rescaling). In all simulations, unbinding forces were increased to achieve an unbinding speed of ~20 m/s (0.20 Å/ps). The time step of the simulation was 1 fs. Data were recorded after the initial equilibration step with configuration-dumping every 1 ps. A Nosé-Hoover thermostat was applied with a thermostat constant of 0.1 ps. All simulations were carried out in vacuum. During the unbinding process, the tethering was reduced to the C_α atoms of every fifth amino acid; the atomic positions were allowed to deviate from the initial position, but with an energy penalty that is a harmonic potential. In half the simulations, the tethering remained unchanged during the whole unbinding process (symmetric tethering). In the remaining simulations, the tethering was lifted from the C_α atoms of these binding-path amino acids (asymmetric tethering), allowing the system more flexibility.

Hydrogen bond analysis

A hydrogen bond can be described as follows: B-A. . . .H-D, where A is an acceptor atom, D is a donor atom, B is an atom immediately bonded to A, and H is a hydrogen atom. The conditions for a hydrogen bond are met when the following criteria are satisfied: 1), the distance between A and D is $<$3.5 Å; 2), the distance between A and H is $<$2.5 Å; 3), the angle subtended by atoms A, H, and D (conventionally known as θ) is between 130° and 180°; and 4), the angle subtended by atoms B, A, and H (conventionally known as ϕ) is between 90° and 180° (20). Note that for acceptor atoms that are bonded to two atoms (such as the nitrogen on histidines), B is a dummy atom created by taking the mean position of the two atoms bonded to nitrogen.

Unbinding pathway

A computer program was written to construct a surface of the unbinding pathway. The algorithm was inspired by an earlier work of Chau and Dean (21). An axis was extended from one end of the pathway to the other end. At regular intervals of 0.25 Å, rays were drawn radially outward, normal to the axis, at angular intervals of every 10°. The point where the ray hits a van der Waals surface of the protein atom is recorded. Together, the collection of such points defines the unbinding tunnel. Cross-sectional areas of the tunnel can also be readily computed at different points along the tunnel axis.

Cell culture and molecular biology

Human embryonic kidney HEK293 cells were grown on 90-mm tissue culture plates at 37°C and 7% CO_2 in a humidified atmosphere. They were cultured in DMEM/F12 (Dulbecco's modified Eagle medium/nutrient mix F12 (1:1)) with GLUTAMAX I containing 10% fetal calf serum, and passaged when confluent. At 70–80% confluency, cells were transfected with mutant or wild-type DNA by electroporation. Mutations were created using the Kunkel method (22) using 5-HT$_{3A(b)}$ subunit DNA (accession AY605711), as described previously (23).

FlexStation assays

These were as previously described (24). Briefly, at 36–48 h posttransfection, cells were washed in flex buffer (115 mM NaCl, 1 mM KCl, 1 mM $CaCl_2$, 1 mM $MgCl_2$, 10 mM glucose, 10 mM HEPES, pH 7.4) and 100 μl of membrane potential dye (Molecular Devices, Wokingham, UK) was added to each well. The plates were incubated at room temperature for 45–60 min before being placed in the FlexStation. Fluorescence was measured every 2 s for a total experimental period of 200 s. At 20 s, 50 μl of either agonist or flex buffer was added to each well.

Softmax Pro (Molecular Devices) or PRISM (Graph Pad, San Diego, CA) was used for data analysis. The percent change in fluorescence, which was calculated as F (peak fluorescence) minus F_0 (baseline fluorescence at 20 s) divided by 5-HT F_{max} (peak fluorescence at 30 μM 5-HT), was compared across 5-HT concentrations using $F = F_{max}/(I + EC_{50}/[5\text{-HT}]^{nH})$, where I is the change in fluorescence, EC_{50} is the concentration required for the half-maximal response, and n_H is the Hill coefficient.

RESULTS

Protein structure

The all-atom root mean-square deviation of the simulated protein structure during the unbinding events is shown in Fig. 2. Data from the initial equilibration are omitted. During the course of the simulation, the protein differed from the original modeled structure by ~2.5 Å, which shows that the protein structure was preserved during the course of unbinding in all eight simulations.

Unbinding trajectories

The trajectories of all eight unbinding simulations are shown in Fig. 3 *A*, where each sphere shows the center of mass of the ligand at 1-ps intervals during the course of unbinding. The trajectories show that both ligands moved along a similar vector that can be described as both downward and outward from the center of the receptor. The trajectories were very similar in the early stages, where the pathway was enclosed by the C-loop, forming a tunnel of ~8 Å in length. The entrance to the tunnel was at the end of the C-loop, ~20 Å above the membrane, and the trajectories deviated from each other beyond this point. Nevertheless, they were all broadly similar, indicating that there was no significant effect of either velocity rescaling or the tethering scheme used. To directly compare the different trajectories, amino acids within 5 Å of the ligand in the course of each trajectory were identified (Tables 1 and 2). These data showed that a total of 52 different amino acids lay on the pathways, and 44% of these were within 5 Å of the ligand in all eight unbinding pathways. These can be considered as consensus residues and

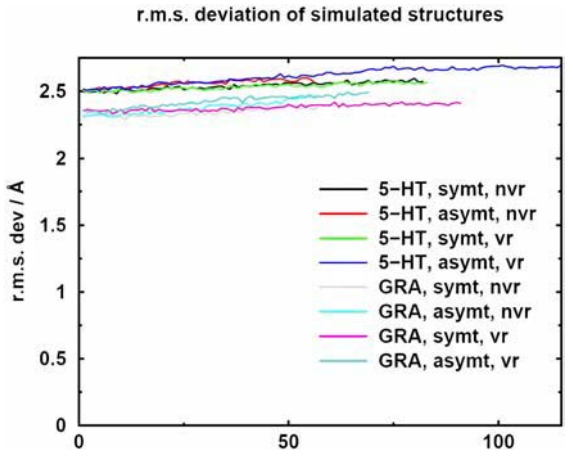

FIGURE 2 Root mean-square deviation of the simulation structure during the course of the experiment, compared to the original model. All atoms are considered in the calculation. GRA, granisetron; asymt, asymmetric tethering; symt, symmetric tethering; nvr, no velocity rescaling, vr, initial velocity rescaling.

their positions are shown in Fig. 3 *B*. The majority of consensus amino acids were located close to the binding pocket, indicating a high degree of conformity in the unbinding trajectories during the early stages of the unbinding process.

To verify that the ligand would only exit the binding site along our proposed exit route, we simulated unbinding of the ligand with the force directed toward the membrane (in the negative *z* direction), inward (toward the ion channel), and outward (away from the ion channel), and the results showed that ligands did not exit the binding site through any other path. Importantly, the ligands still followed the same trajectories as those described above (data not shown).

Unbinding of 5-HT

The amino acids we previously identified as being within 5 Å of 5-HT in its correct orientation in the binding site are marked in Table 1 (taken from model 4 of Reeves et al. (15)). As expected, these amino acids interacted with the ligand at the early stages of the simulation (*white squares*) but not at the latter stages (*black squares*). Three overlapping frames of the position of 5-HT at 0 ps, 48 ps, and 56 ps into the simulation (Fig. 4) show that the unbinding pathway follows the tunnel described above. Forty-three amino acids were identified as being on the 5-HT unbinding pathways, with 74% of these present in all four pathways.

The hydrogen-bonding pattern between the ligand and the receptor on the exit pathway are shown in Table 3. The hydrogen-bonding profiles of the four 5-HT trajectories were qualitatively similar, so we have only presented the data for 5-HT unbinding from a symmetrically tethered protein with no initial velocity rescaling. In the initial stages, the hydrogen bonds formed between the ligand and the receptor were similar to those reported in the literature (25). As the ligand left the binding site, it turned slightly so that these interactions were replaced by other hydrogen bonds. Of these, the most persistent were those with E236, which initially acted as a hydrogen-bond acceptor with the H_η of 5-HT, then H_{N2}, and finally H_{N3}; Y153, which acts as a hydrogen-bond acceptor first to H_{N2} and then to H_{N1} of 5-HT; W183, which acts as an acceptor to H_{N1}, H_{N2}, and then H_{N3} of 5-HT; K238, which acts as a donor to the O of 5-HT; and E129, which hydrogen-bonds with H_{N1} and then with H_{N3}. Thus, some of the amino acids contributing to the hydrogen bonds are in the enclosed part of the unbinding pathway, whereas others lie in the groove that extends from this enclosed region toward the membrane. There are no explicit waters in our simulations, but given the size of 5-HT and the volume of the binding pocket, it is unlikely that water would exist in this site.

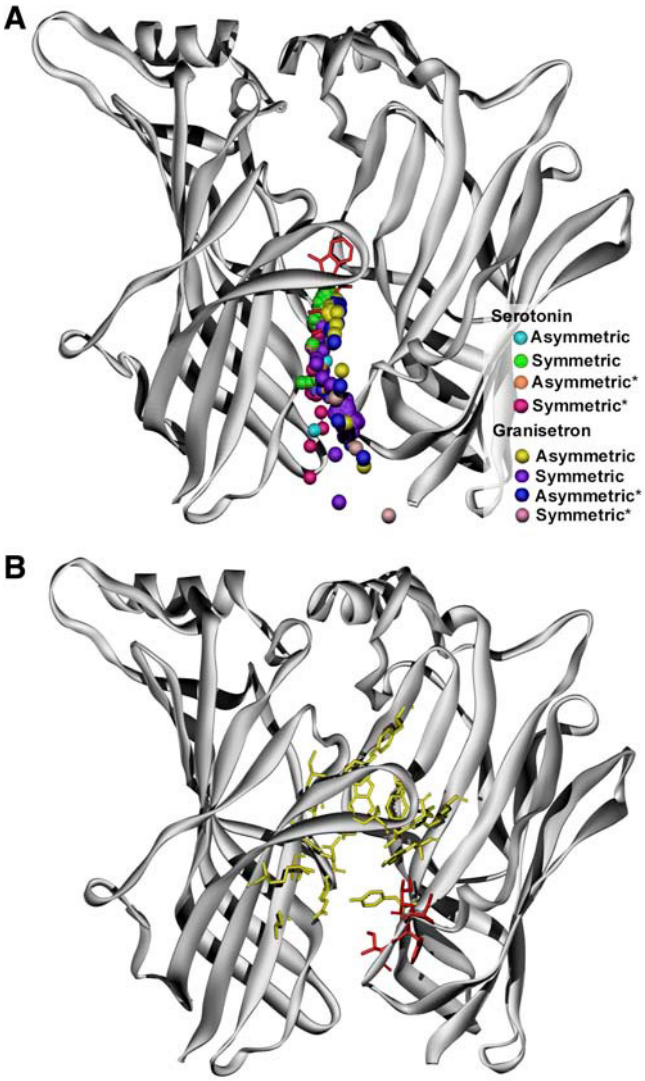

FIGURE 3 Unbinding trajectories and consensus amino acids in the 5-HT_3 unbinding pathway. (*A*) Unbinding trajectories for 5-HT and granisetron. Spheres represent the centers of mass of the ligand. All eight simulations performed in this study are shown. (*B*) Residues from early (*yellow*) and late (*red*) stages of the unbinding simulation. Residues within this figure are shown in Tables 1 and 2.

TABLE 1 Comparison of amino acids that lie within 5 Å of 5-HT along the unbinding pathway

		5-HT			
Loop	Residue	Symmetric tethering	*Symmetric tethering	Asymmetric tethering	*Asymmetric tethering
	Q83	■	■		■
	L126				
A	N128†	□	□	□	□
	E129	□	□	□	□
	F130		□		
	C162	■	■	■	■
	S163	■	■	■	■
	L164	■	■	■	■
	D165	■	■		
	I166	■	■		
	Y167	■	■		
	N174	■	■		■
	S177	□	□	□	□
	T179†	□	□	□	□
B	T181†	□	□	□	□
	S182†	□	□	□	□
	W183†	□	□	□	□
	L184†	□	□	□	□
	H185	□			
	K224	□	□	□	□
	E225				
	F226†	□	□	□	□
	S227				
	I228†	□	□	□	□
	D229	□	□	□	□
C	I230	□	□	□	□
	S231				
	N232				
	S233				
	Y234†	□	□	□	□
	A235	□			
	E236†	□	□	□	□
	K238	□	□	□	□
	Y240	■	■	■	■
	I71	□	□	□	□
	Y73	□	□	□	□
D	W90†	□	□	□	□
	R92†	□	□	□	□
E	Y143†	□	□	□	□
	Y153†	□	□	□	□
	L156			□	□
	V201				
	R202				
	S203				
	K205		■		■
F	S206	■	■	■	■
	I207	■	■	■	■
	F208	■	■	■	■
	I209	■	■	■	■
	N210	■	■	■	■
	Q211	■	■	■	■
	G212	■			
Unbinding speed (m/s)		21	20	27	14

Residues present within the binding site during the early stages of the simulation are shown as white squares and later residues are shown as black squares. These residues are also shown in Fig. 1. Residues that remain unhighlighted were identified in granisetron unbinding simulations, but were not identified during 5-HT unbinding. Average unbinding speeds for the full trajectory of each simulation are shown in the bottom row of each column.

*Velocity rescaling was performed on these simulations.

†Amino acids previously identified as binding-site residues (15).

TABLE 2 Comparison of amino acids that lie within 5 Å of granisetron along the unbinding pathway

		Granisetron			
Loop	Residue	Symmetric tethering	*Symmetric tethering	Asymmetric tethering	*Asymmetric tethering
	Q83	■			
	L126			□	
A	N128	□	□	□	□
	E129†	□	□	□	□
	F130				
	C162	■			
	S163	■			
	L164	■	■		■
	D165				
	I166				
	Y167				
	N174				
	S177	□	□	□	□
	T179†	□	□	□	□
	T181†	□	□	□	□
B	S182†	□	□	□	□
	W183†	□	□	□	□
	L184†		□	□	□
	H185				
	K224			□	□
	E225	□			
	F226	□	□	□	□
	S227	□	□	□	□
	I228†	□	□	□	□
	D229†	□	□	□	□
C	I230†	□	□	□	□
	S231		□	□	□
	N232		□	□	□
	S233				□
	Y234†	□	□	□	□
	A235	□			
	E236	□	□	□	□
	K238	□	□	□	□
	Y240				
	I71			□	□
	Y73	□	□	□	□
D	W90†	□	□	□	□
	R92†	□	□	□	□
E	Y143	□	□	□	□
	Y153†	□	□	□	□
	L156		□	□	□
	V201	□	□	□	□
	R202	□	□	□	□
	S203	■			
	K205	■	■	■	■
	S206†	■	■	■	■
F	I207	■	■	■	■
	F208	■	■	■	■
	I209	■	■	■	■
	N210	■	■	■	
	Q211	■			
	G212				
Unbinding speed (m/s)		35	19	35	30

Residues that were present within the binding site during the early stages of the simulation are shown as white squares and later residues are shown as black squares. These residues are also shown in Fig. 1. Residues that remain unhighlighted were seen in 5-HT unbinding simulations, but were not identified during granisetron unbinding. Average unbinding speeds for the full trajectory of each simulation are shown in the bottom row of each column.

*Velocity rescaling was performed on these simulations.

†Amino acids previously identified as binding-site residues (15).

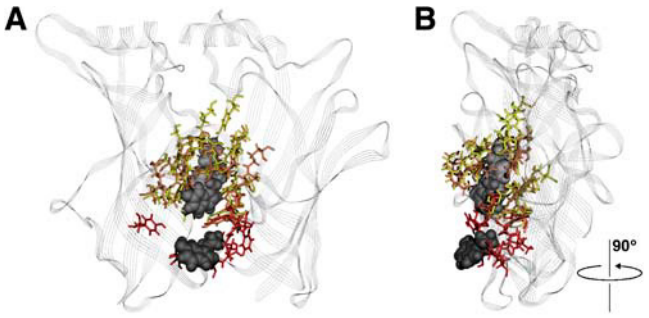

FIGURE 4 Movement of 5-HT during an unbinding simulation. For ease of viewing only two subunits from the pentamer are shown. (*A*) A view from the front of two adjacent subunits showing 5-HT at 0-ps (*white ligand*, *yellow amino acids*), 48-ps (*light gray ligand*, *orange amino acids*) and 56-ps (*dark gray ligand*, *red amino acids*) time intervals and highlighting that the ligand moves both down and out during the unbinding process. (*B*) A side view of the unbinding sequence shown in panel *A*.

Unbinding of granisetron

The amino acid residues identified as being within 5 Å of docked granisetron in its correct orientation (19) are indicated in Table 2. Similar to 5-HT unbinding, these residues are seen to interact with the ligand in the early, but not the late, stages of the simulation. The sole exception is residue S206. This is interesting as it is located on the F-loop whose position in the high-resolution structure of AChBP has not yet been finalized. However, it is clear from our previous studies that it plays a role in the binding and/or function of the receptor (19) and our current data support this. Three overlapping frames of the position of granisetron at 0 ps, 10 ps, and 55 ps into the simulation show that the unbinding pathway is similar to that for 5-HT (Fig. 5). In total, 44 residues were located on the granisetron unbinding pathways, with 59% found in all four pathways.

The hydrogen bonds between granisetron and its receptor during the course of unbinding are shown in Table 4. Similar to 5-HT, the hydrogen-bonding profiles of the four granisetron trajectories were qualitatively similar, so we have only presented the data for granisetron unbinding from an asymmetrically tethered protein with initial velocity rescaling. It can be seen that granisetron establishes fewer hydrogen bonds than 5-HT, perhaps because these are less important for an antagonist as compared to an agonist. Throughout the simulation, there were only three hydrogen bonds and these were between the hydrogen linked to the amide nitrogen of granisetron and the $O_{\delta 1}$ of N128, between the indazole nitrogen of granisetron and the hydroxyl group of Y153, and the ammonium hydrogen of the azabicyclic ring and the main-chain oxygen of I207.

Unbinding pathway

A reconstruction of the unbinding pathway from the original homology model is shown in Fig. 6. Fig. 6, *left*, shows the surface of the unbinding pathway looking from the extracellular environment toward the outer surface of the 5-HT$_3$ receptor, and Fig. 6, *right*, shows a cross-sectional area of the pathway at different positions along its length. From the top of the binding site, the pathway widens to a maximum of $\sim$120 Å^2 at the location of Y153, constricts at the level of I228, and then widens toward the mouth of the pathway. As it proceeds closer to the membrane, the C-loop ends and the tunnel that was present in the initial stages of the unbinding process becomes a groove. The text and arrows in the center of Fig. 6 show the location of the views in Fig. 7.

Comparison with previous docking models

The unbinding pathway is supported by our previous findings from docking granisetron into the binding site (19). In these studies, 13 energetically favorable models were created and were found to fall into three main groups based upon the orientation of granisetron in the binding site. Fig. 8 shows the position and orientation of granisetron in the three model types. In model types A (Fig. 8 *A*) and B (Fig. 8 *B*), the location of granisetron is broadly similar, with granisetron docked high in the binding site, although the azabicyclic ring is located at different ends of the binding pocket. In model type C (Fig. 8 *C*), granisetron is located outside the binding pocket in a region significantly closer to the membrane. A comparison of residues in model types A and B (*yellow*) and model type C (*red*) is shown in Fig. 8 *D* (common residues are shown in *orange*). Amino acids within models A and B were almost all identified as residues that interacted in the ''early'' part of the granisetron unbinding simulation, whereas amino acid residues close to the ligand in model type C interact with the ligand later in the simulation. This indicates that the potential binding site of granisetron shown in model C is located on the unbinding pathway (Fig. 5).

Functional assays

Hydrogen-bonding data from the simulation study (Table 3) showed that residues E236, W183, Y153, and K238 spent the highest proportion of the total simulation time (27–47%) bonding with 5-HT as it exited the binding site. Some radioligand binding and functional data is already available for receptors mutated at these positions and these data show large changes in binding and functional properties of W183A and Y153A mutant receptors (19,26–29). As the side chain on alanine cannot form hydrogen bonds, these data are consistent with our hypothesis that these residues may hydrogen-bond to 5-HT. Radioligand binding data are also available for E236A and K238A mutant receptors and show no change in binding affinity compared to wild-type receptors (19). However, our current data show large changes in EC_{50} in both mutant receptors: E236A mutant receptors did not function at concentrations up to 100 μM 5-HT, and K238A-containing receptors had a 10-fold shift in EC_{50} (1.36 μM,

TABLE 3 Hydrogen bonds between amino acid residues along the ligand unbinding pathway and 5-HT

Hydrogen bond acceptor	Acceptor atom	Hydrogen bond donor	Donor atom
Y153	O_{η}	5-HT	H_{N2}
E236	$O_{\varepsilon 1}$	5-HT	H_{η}
5-HT	O	K238	$H_{\zeta 1}$
W183	O	5-HT	H_{N1}
W183	O	5-HT	H_{N2}
W183	O	5-HT	H_{N3}
E236	$O_{\varepsilon 2}$	5-HT	H_{η}
Y234	O_{η}	5-HT	H_{N3}
Y153	O_{η}	5-HT	H_{N3}
Y234	O_{η}	5-HT	H_{N1}
5-HT	O	K238	$H_{\zeta 2}$
T181	$O_{\gamma 1}$	5-HT	H_{N2}
5-HT	O	K238	$H_{\zeta 3}$
E236	$O_{\varepsilon 1}$	5-HT	H_{N2}
T181	$O_{\gamma 1}$	5-HT	H_{N3}
E129	$O_{\varepsilon 2}$	5-HT	H_{N1}
E236	$O_{\varepsilon 2}$	5-HT	H_{N3}
S206	O	5-HT	$H_{\varepsilon 1}$
E236	$O_{\varepsilon 1}$	5-HT	H_{N3}
S163	O	5-HT	H_{η}
5-HT	O	Q211	$H_{\varepsilon 22}$
5-HT	O	Q211	$H_{\varepsilon 21}$
E129	$O_{\varepsilon 1}$	5-HT	H_{N3}
S163	O	5-HT	H_{N1}
Q83	$O_{\varepsilon 1}$	5-HT	H_{η}
5-HT	O	Q83	$H_{\varepsilon 22}$

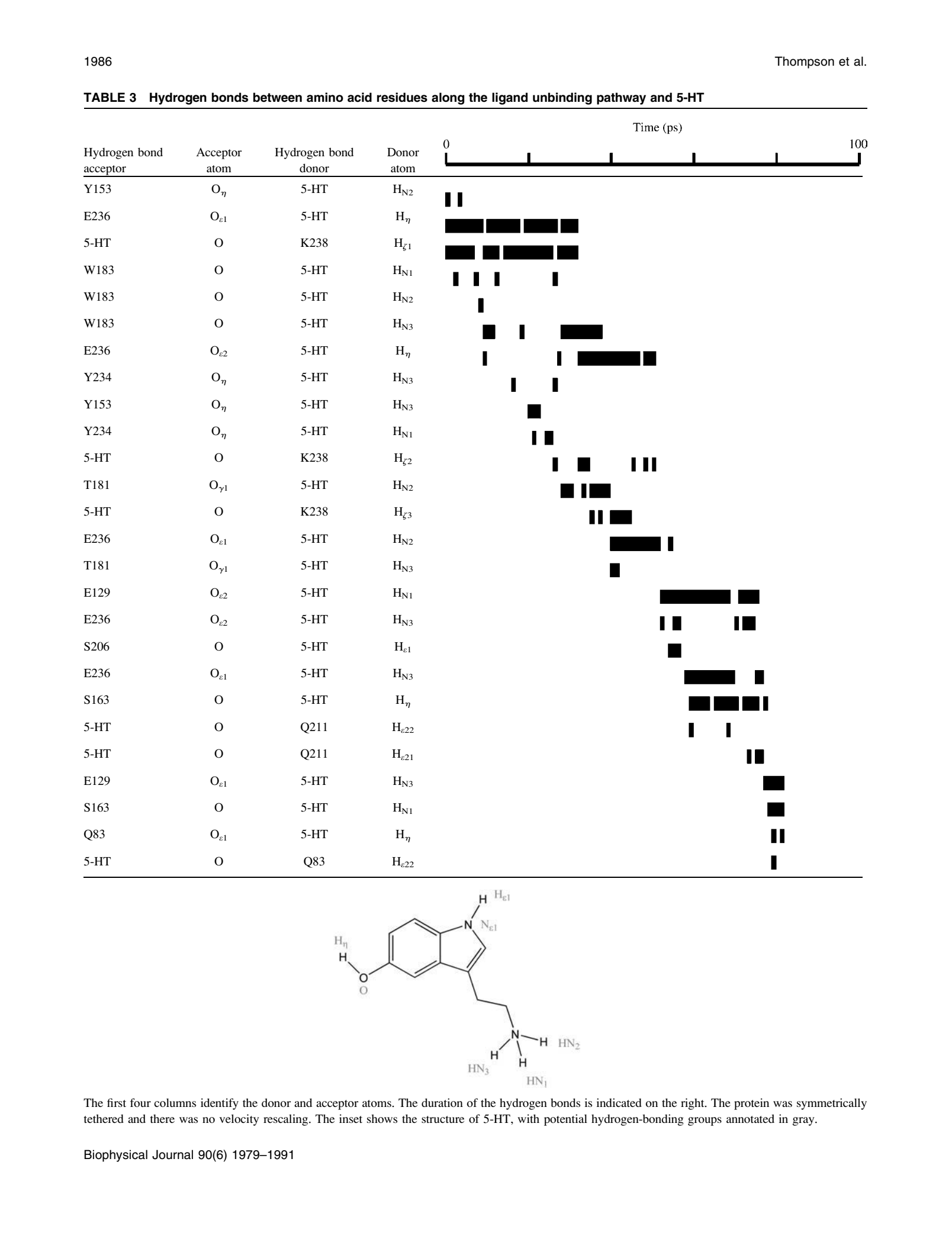

The first four columns identify the donor and acceptor atoms. The duration of the hydrogen bonds is indicated on the right. The protein was symmetrically tethered and there was no velocity rescaling. The inset shows the structure of 5-HT, with potential hydrogen-bonding groups annotated in gray.

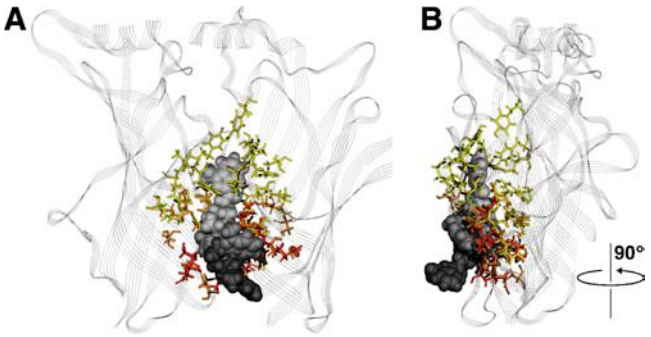

FIGURE 5 Movement of granisetron during an unbinding simulation. For ease of viewing, only two subunits from the pentamer are shown. (*A*) A view from the front of two adjacent subunits showing granisetron at 0-ps (*white ligand*, *yellow amino acids*), 10-ps (*light gray ligand*, *orange amino acids*), and 55-ps (*dark gray ligand*, *red amino acids*) time intervals. Similar to 5-HT (Fig 4), the ligand moves both down and out during the unbinding process. (*B*) A side view of the unbinding sequence shown in panel *A*.

compared to 0.2 μM for wild-type receptors). As EC_{50} is a term that encompasses both binding and functional parameters, these data suggest that agonist binding or function is impaired. They therefore support our hypothesis that hydrogen bonding with the agonist is important. Some hydrogen bonding was also indicated between 5-HT and T181, S206, Y234, E129, Q211, S163, and Q83. Examination of receptor function when each of these residues was replaced by alanine suggests that they may also hydrogen-bond to 5-HT: E129A, Q83A, and S206A mutant receptors were nonfunctional up to 100 μM 5-HT, Y234A mutation caused a 70-fold increase in EC_{50} (23), and T181A resulted in a 10-fold increase (EC_{50} = 1.95 μM). Q211A and S163A mutant receptors had EC_{50} values similar to wild-type receptors (0.17 and 0.24 μM, respectively). These data are shown in Fig. 9.

DISCUSSION

This study has used molecular dynamics simulations to provide a qualitative insight into the locations of both an agonist and an antagonist as they exit the binding site of the 5-HT$_3$ receptor. The data revealed that the exit pathway is a tunnel formed at the interface of two subunits, which is almost vertical with respect to the plane of the membrane. It is ~8 Å long and its entrance is ~20 Å above the membrane. These data are supported by functional studies.

The model that we have used to determine the unbinding pathway is the homology model of the 5-HT$_3$ receptor, which is based on the structure of AChBP. AChBP has considerable structural similarity with the extracellular domain of the nACh receptor, and is a good template for the closely related 5-HT$_3$ receptor. However, as our data are based on a model and not on an atomic resolution structure, caution must be applied in interpreting molecular details. Indeed, until a high-resolution structure is available, such studies can only provide qualitative information, although some details of molecular interactions can be obtained from experimental studies. We have previously used such studies to show that the predicted structure of the binding site is reasonably accurate: Mutagenesis has demonstrated that many key residues

TABLE 4 Hydrogen bonds between amino acid residues along the ligand unbinding pathway and granisetron

Hydrogen bond acceptor	Acceptor atom	Hydrogen bond donor	Donor atom	Time (ps) 0 — 100
I207	O	Granisetron	$H_{\kappa 1}$	
Granisetron	$N_{\delta 1}$	Y153	H_{η}	
N128	$O_{\delta 1}$	Granisetron	H_{γ}	

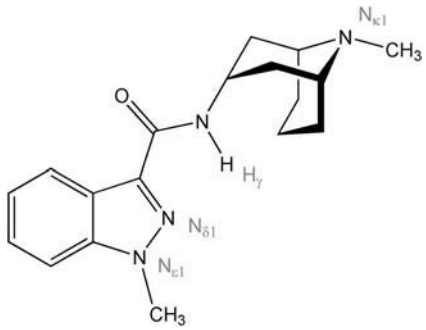

The first four columns identify the donor and acceptor atoms. The duration of the hydrogen bonds is indicated on the right. The protein was symmetrically tethered and there was no velocity rescaling. The inset shows the structure of granisetron, with potential hydrogen-bonding groups annotated in gray.

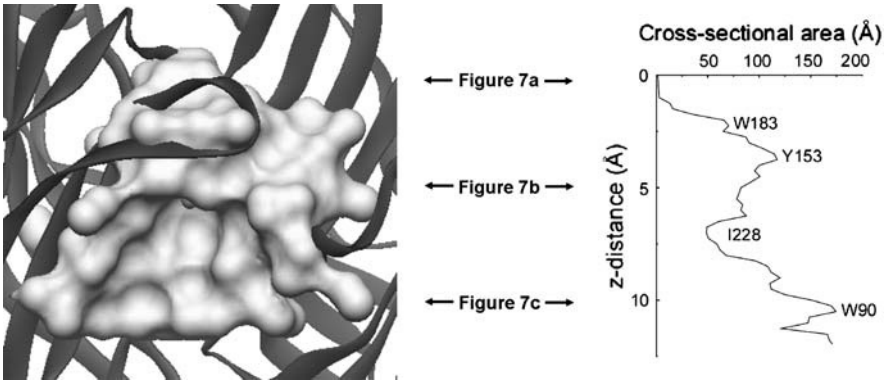

FIGURE 6 Surface and cross-sectional area of the unbinding pathway of the original homology model. (*Left*) The surface of the unbinding pathway is shown as viewed from the extracellular environment, looking toward the C-loop of the receptor. (*Right*) Cross-sectional area of the ligand unbinding pathway immediately after the initial 100-ps equilibration of 5-HT in the ligand binding site. Text and arrows indicate the locations of the views shown in Fig 7.

identified in the binding pocket affect agonist and/or antagonist binding to the receptor. The roles of W183, Y143, Y153, and Y234 have been particularly well studied, and these data have shown that these residues form hydrogen bonds and/or cation-π interactions with ligands (15,19,26,28). Further studies in which all 26 residues proposed to form the binding site were mutated provide yet more support for the model (19).

The 5-HT_3 receptor, like all Cys-loop receptors, exists in a number of conformations, including an open, a closed, and one or more desensitized states. It is not yet known how much the structure of the protein varies in these different states, although significant changes in the nACh receptor have been reported (30). AChBP has been proposed to be similar to the open or desensitized state of the nACh receptor, and the location of residues that interact with 5-HT when it is docked into the binding site of the AChBP-based homology model are well supported by experimental evidence, so our positioning of 5-HT in the binding site is probably fairly accurate (1,2,31). Therefore, taking into account the limitations mentioned above, the unbinding pathway that we have identified is probably as accurate as the structure and the molecular simulations allow, although, as the closed state of the receptor has a distinct structure, it is probably not a good representation of the binding pathway. A recent study by Unwin (4) shows that in the resting state of the nACh receptor, the C-loop points away from the center of the receptor, ''opening'' the binding-site pocket and making it more accessible. Consequently, it is possible that ligands have a number of potential routes into the binding site, and indeed, in the $GABA_A$ receptor it has been proposed that the ligand accesses the binding site from the side (32). Maksay et al. (25) alluded to the region we have identified as the entry point of the ligand into the binding site (see Fig. 4 in that article) but the new structural information better supports ligands having a fairly unrestricted access (6). This is entirely reasonable, as entry to the binding site must be rapid to allow opening of the channel within milliseconds of agonist application, whereas ligand unbinding is in the hundreds of milliseconds to seconds time range (33–35). Structural data suggest that in the ligand-bound conformation the C-loop has closed over the ligand, restricting access to the binding site and leaving only a narrow passage through which the ligand can exit (Fig. 3). This exit route would place the ligand some distance from the binding pocket and, we speculate, would prevent immediate reentry of the ligand to the binding site when the receptor reverts to the closed conformation.

There are as yet no high-resolution structural details of the ligand binding pocket of any Cys-loop receptor with antagonist bound. However, in the 5-HT_3 receptor we anticipate that this structure would be more similar to the open than to the closed state, as our docking studies of granisetron in the AChBP-like (open state) homology model are well supported by experimental evidence (19). We therefore believe that the starting location for granisetron that we used for the simulations is broadly correct and that the pathway we have identified is qualitatively accurate, although some molecular details may vary. Support for this hypothesis comes from docking studies with granisetron, where a potential binding site for this molecule was located on the unbinding pathway (19). A further binding site for another 5-HT_3 antagonist (tetrahydroacridine) has also been located on our proposed pathway (36).

Of the residues thought to participate in the latter part of the unbinding pathway, only S206 has previously been shown to affect antagonist binding affinity when mutated, suggesting a role in binding and/or function of the 5-HT_3 receptor (19). It is known from structural studies that this residue is located within the F-loop, which is a flexible region in AChBP. F-loop residues have also been shown to play a role in $GABA_A$ and nACh receptor function (37–39) and consequently it is not surprising that mutations in this region also have an effect on 5-HT_3 receptor function. Structural details of the F-loop region are poorly resolved in the crystal structures of the AChBP (1,2) and in cryoelectron microscopy images of the nACh receptor (6), suggesting that the homology models may be inaccurate in this region. However, there is increasing evidence from mutagenesis and functional studies that this region undergoes structural changes upon ligand binding.

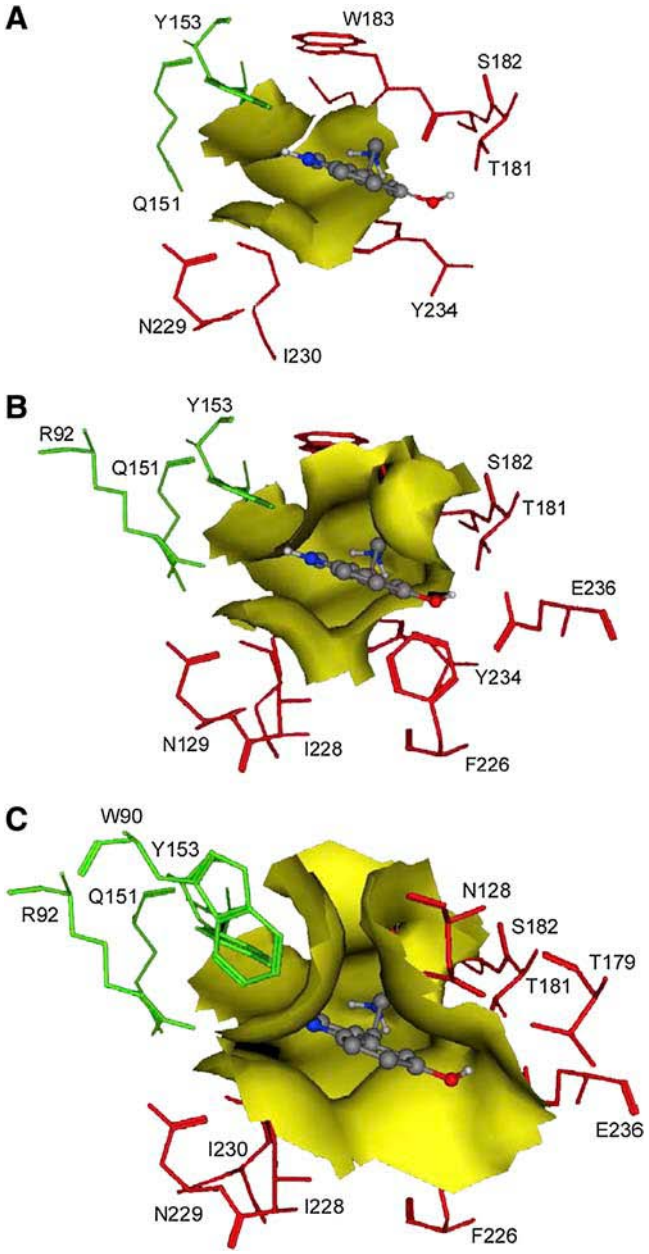

FIGURE 7 Views of the unbinding pathway taken at different locations along the unbinding trajectory. Images are representative of views taken at 3.5 Å (at the level of Y153), 6.5 Å (I228), and 10.5 Å (W90) from the terminating residue located in the binding site. The positions from which these views were taken are shown in Fig 6 and are shown immediately before unbinding, with 5-HT located in the binding site of the equilibrated receptor.

The tunnel that forms the exit route is considerably shorter than the binding ''gorge'' described by Sussman et al. (5) in acetylcholinesterase. This might be expected, as in a ligand-gated receptor a neurotransmitter must be able to enter and exit the binding site more rapidly than a substrate or product of an enzymic reaction. Interestingly, both the active site gorge and Cys-loop receptor binding sites are

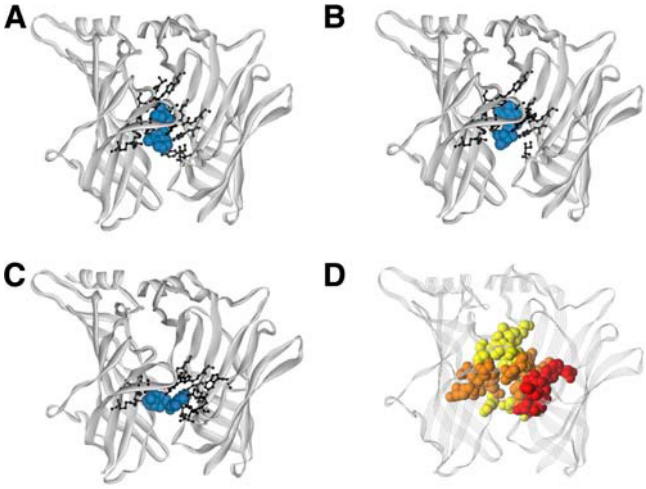

FIGURE 8 (*A–C*) Comparison of residues within 5 Å of the ligand binding site from docked-pose clusters of models A, B, and C from Thompson et al. (18). Granisetron is shown in blue. (*D*) A comparison of residues that are involved with the docked-pose clusters A and B (*yellow*) and cluster C (*red*). Residues that are common to both groups are highlighted in orange.

dominated by aromatic amino acids, although there are lower proportions of this type of amino acid in the unbinding pathway, suggesting that hydrophobic interactions have less importance here. However, there are many potential hydrogen bonding partners for 5-HT on the neurotransmitter unbinding pathway. Mutation of those amino acids that dominate the hydrogen-bonding pattern show that they play an important role in receptor function. These data provide support for the pathway and also suggest that these bonds may be more important than aromatic interactions for the movement of the ligand in this protein.

In conclusion, we have defined a potential unbinding pathway for ligands from the 5-HT$_3$ receptor binding pocket using molecular dynamics simulations. The routes of both an agonist and an antagonist were similar, extending from the ligand binding site down toward the membrane. From these and other functional and structural data, we propose the following model. The ligand enters the binding site from one of several possible directions owing to the open nature of the binding pocket in the extended C-loop conformation. Ligand binding pulls the C-loop across the pocket, closing access to the site, and, in the case of an agonist, initiating a series of events that lead to channel opening and subsequent receptor desensitization. The ligand then leaves the binding pocket through the base of the binding site, along the only pathway that remains unobstructed after the movements of the extracellular domain. This places the ligand some distance from the binding site and the protein undergoes a conformational change back into the closed, resting state.

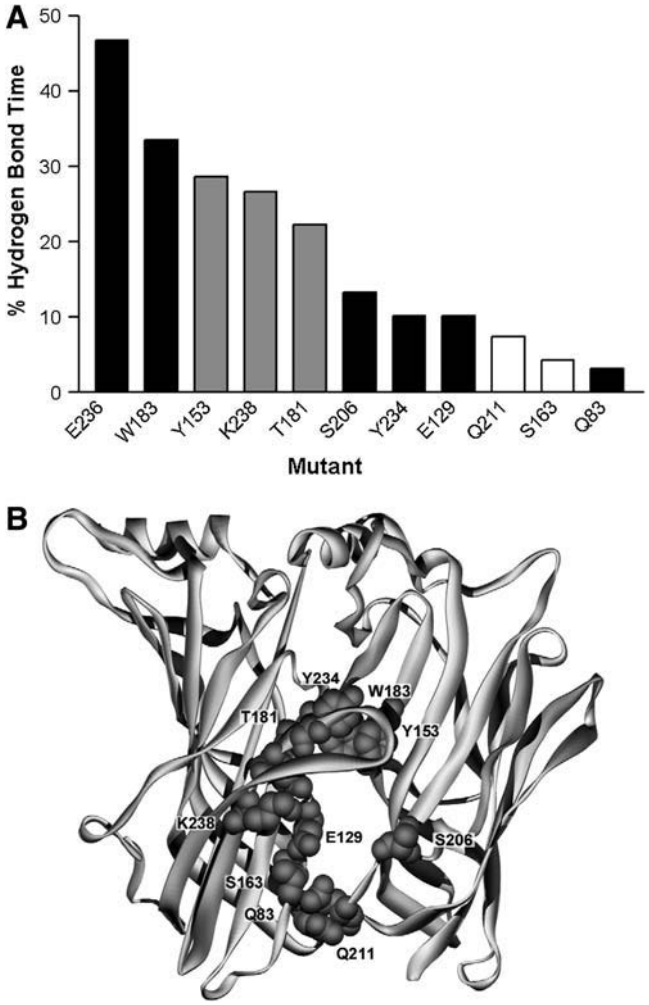

FIGURE 9 Experimental study of the residues that have been shown to hydrogen-bond with 5-HT during the unbinding simulation. (*A*) Percentage of the total unbinding time that the residues are hydrogen-bonded with 5-HT as it exits along the unbinding pathway (from data shown in Table 3). Black bars indicate the receptor is nonfunctional, gray bars indicate an increase in the EC_{50} relative to wild-type receptors, and white bars indicate an EC_{50} similar to that of wild-type. (*B*) The location of the residues in panel *A* are shown on a model of the 5-HT_3 extracellular domain. For clarity, only two of the five subunits required for a functional receptor are shown.

A.J.T. and S.C.R.L. are supported by the Wellcome Trust. S.C.R.L. is a Wellcome Trust Senior Research Fellow in Basic Biomedical Sciences. P.-L.C. and S.C.R.L. thank the Royal Society for a European Scientific Exchange Program travel grant.

REFERENCES

1. Celie, P. H., S. E. van Rossum-Fikkert, W. J. van Dijk, K. Brejc, A. B. Smit, and T. K. Sixma. 2004. Nicotine and carbamylcholine binding to nicotinic acetylcholine receptors as studied in AChBP crystal structures. *Neuron*. 41:907–914.
2. Brejc, K., W. J. van Dijk, R. V. Klaassen, M. Schuurmans, J. van Der Oost, A. B. Smit, and T. K. Sixma. 2001. Crystal structure of an ACh-binding protein reveals the ligand-binding domain of nicotinic receptors. *Nature*. 411:269–276.
3. Bouzat, C., F. Gumilar, G. Spitzmaul, H. L. Wang, D. Rayes, S. B. Hansen, P. Taylor, and S. M. Sine. 2004. Coupling of agonist binding to channel gating in an ACh-binding protein linked to an ion channel. *Nature*. 430:896–900.
4. Unwin, N. 2005. Refined structure of the nicotinic acetylcholine receptor at 4Å resolution. *J. Mol. Biol.* 346:967–989.
5. Sussman, J. L., M. Harel, F. Frolow, C. Oefner, A. Goldman, L. Toker, and I. Silman. 1991. Atomic structure of acetylcholinesterase from *Torpedo californica*: a prototypic acetylcholine-binding protein. *Science*. 253:872–879.
6. Miyazawa, A., Y. Fujiyoshi, M. Stowell, and N. Unwin. 1999. Nicotinic acetylcholine receptor at 4.6 Å resolution: transverse tunnels in the channel wall. *J. Mol. Biol.* 288:765–786.
7. Kern, P., R. M. Brunne, and G. Folkers. 1994. Nucleotide-binding properties of adenylate kinase from *Escherichia coli*—a molecular-dynamics study in aqueous and vacuum environments. *J. Comput. Aided Mol. Des.* 8:367–388.
8. Rognan, D., L. Scapozza, G. Folkers, and A. Daser. 1994. Molecular dynamics simulation of MHC-peptide complexes as a tool for predicting potential T cell epitopes. *Biochemistry*. 33:11476–11485.
9. Leech, J., J. Prins, and J. Herma. 1996. SMD: visual steering of molecular dynamics for protein design. *IEEE Comput. Sci. Eng.* 3: 38–45.
10. Izrailev, S., S. Stepaniants, M. Balsera, Y. Oono, and K. Schulten. 1997. Molecular dynamics study of unbinding of the avidin-biotin complex. *Biophys. J.* 72:1568–1581.
11. Marrink, S. J., O. Berger, P. Tieleman, and F. Jähnig. 1998. Adhesion forces of lipids in a phospholipid membrane studied by molecular dynamics simulations. *Biophys. J.* 74:931–943.
12. Kosztin, D., S. Izrailev, and K. Schulten. 1999. Unbinding of retinoic acid from its receptor studied by steered molecular dynamics. *Biophys. J.* 76:188–197.
13. Grubmüller, H., B. Heymann, and P. Tavan. 1996. Ligand binding: molecular mechanics calculation of the streptavidin-biotin rupture force. *Science*. 271:997–999.
14. Chau, P.-L. 2001. Process and thermodynamics of ligand-receptor interaction studied using a novel simulation method. *Chem. Phys. Lett.* 334:343–351.
15. Reeves, D. C., M. F. Sayed, P. L. Chau, K. L. Price, and S. C. Lummis. 2003. Prediction of 5-HT_3 receptor agonist-binding residues using homology modeling. *Biophys. J.* 84:2338–2344.
16. Sali, A., and T. L. Blundell. 1993. Comparative protein modelling by satisfaction of spatial restraints. *J. Mol. Biol.* 234:779–815.
17. Smith, W., and T. R. Forester. 1996. DL_POLY_2.0: a general-purpose parallel molecular dynamics simulation package. *J. Mol. Graph.* 14:136–141.
18. MacKerell, A. D., D. Bashford, M. Bellott, R. L. Dunbrack, J. D. Evanseck, M. J. Field, S. Fischer, J. Gao, H. Guo, S. Ha, D. Joseph-McCarthy, L. Kuchnir, et al. 1998. All-atom empirical potential for molecular modeling and dynamics studies of proteins. *J. Phys. Chem. B*. 102:3586–3616.
19. Thompson, A. J., K. L. Price, D. C. Reeves, S. L. Chan, P. L. Chau, and S. C. Lummis. 2005. Locating an antagonist in the 5-HT_3 receptor binding site using modeling and radioligand binding. *J. Biol. Chem.* 280:20476–20482.
20. Chau, P.-L., T. R. Forester, and W. Smith. 1996. Curvature effects in hydrophobic solvation. *Mol. Phys.* 89:1033–1055.
21. Chau, P.-L., and P. M. Dean. 1987. Molecular recognition: 3D surface structure comparison by gnomonic projection. *J. Mol. Graph.* 5: 97–100.
22. Kunkel, T. A. 1985. Rapid and efficient site-specific mutagenesis without phenotypic selection. *Proc. Natl. Acad. Sci. USA*. 82:488–492.
23. Hargreaves, A. C., M. J. Gunthorpe, C. W. Taylor, and S. C. Lummis. 1996. Direct inhibition of 5-hydroxytryptamine3 receptors by antagonists of L- type Ca^{2+} channels. *Mol. Pharmacol.* 50:1284–1294.

24. Price, K. L., and S. C. Lummis. 2005. FlexStation examination of 5-HT_3 receptor function using Ca^{2+} - and membrane potential-sensitive dyes: advantages and potential problems. *J. Neurosci. Methods.* 149:172–177.

25. Maksay, G., Z. Bikadi, and M. Simonyi. 2003. Binding interactions of antagonists with 5-hydroxytryptamine3A receptor models. *J. Recept. Signal Transduct. Res.* 23:255–270.

26. Spier, A. D., and S. C. Lummis. 2000. The role of tryptophan residues in the 5-Hydroxytryptamine(3) receptor ligand binding domain. *J. Biol. Chem.* 275:5620–5625.

27. Price, K. L., and S. C. Lummis. 2004. The role of tyrosine residues in the extracellular domain of the 5-hydroxytryptamine3 receptor. *J. Biol. Chem.* 279:23294–23301.

28. Beene, D. L., K. L. Price, H. A. Lester, D. A. Dougherty, and S. C. Lummis. 2004. Tyrosine residues that control binding and gating in the 5-hydroxytryptamine3 receptor revealed by unnatural amino acid mutagenesis. *J. Neurosci.* 24:9097–9104.

29. Beene, D. L., G. S. Brandt, W. Zhong, N. M. Zacharias, H. A. Lester, and D. A. Dougherty. 2002. Cation-π interactions in ligand recognition by serotonergic (5-HT_{3A}) and nicotinic acetylcholine receptors: the anomalous binding properties of nicotine. *Biochemistry.* 41:10262–10269.

30. Unwin, N., A. Miyazawa, J. Li, and Y. Fujiyoshi. 2002. Activation of the nicotinic acetylcholine receptor involves a switch in conformation of the α-subunits. *J. Mol. Biol.* 319:1165–1176.

31. Celie, P. H., R. V. Klaassen, S. E. van Rossum-Fikkert, R. van Elk, P. van Nierop, A. B. Smit, and T. K. Sixma. 2005. Crystal structure of AChBP from *Bulinus truncatus* reveals the conserved structural scaffold and sites of variation in nicotinic acetylcholine receptors. *J. Biol. Chem.* 280:26457–26466.

32. Berezhnoy, D., Y. Nyfeler, A. Gonthier, H. Schwob, M. Goeldner, and E. Sigel. 2004. On the benzodiazepine binding pocket in $GABA_A$ receptors. *J. Biol. Chem.* 279:3160–3168.

33. Suprenant, A., and J. Crist. 1988. Electrophysiological characterization of functionally distinct 5-hydroxytryptamine receptors on guinea-pig submucous plexus. *Neuroscience.* 24:283–295.

34. Yakel, J. L., and M. B. Jackson. 1988. 5-HT3 receptors mediate rapid responses in cultured hippocampus and a clonal cell line. *Neuron.* 1:615–621.

35. Maricq, A. V., A. S. Peterson, A. J. Brake, R. M. Myers, and D. Julius. 1991. Primary structure and functional expression of the $5HT_3$ receptor, a serotonin-gated ion channel. *Science.* 254:432–437.

36. Camilleri, M. 2001. Management of the irritable bowel syndrome. *Gastroenterology.* 120:652–668.

37. Newell, J. G., and C. Czajkowski. 2003. The $GABA_A$ receptor α 1 subunit Pro174-Asp191 segment is involved in GABA binding and channel gating. *J. Biol. Chem.* 278:13166–13172.

38. Martin, M., C. Czajkowski, and A. Karlin. 1996. The contributions of aspartyl residues in the acetylcholine receptor γ and δ subunits to the binding of agonists and competitive antagonists. *J. Biol. Chem.* 271:13497–13503.

39. Sedelnikova, A., C. D. Smith, S. O. Zakharkin, D. Davis, D. S. Weiss, and Y. Chang. 2005. Mapping the rho1 $GABA_C$ receptor agonist binding pocket. Constructing a complete model. *J. Biol. Chem.* 280:1535–1542.